Physics Letters B 693 (2010) 575–579

Contents lists available at ScienceDirect

Physics Letters B

www.elsevier.com/locate/physletb

Kinematic cusps: Determining the missing particle mass at colliders

Tao Han [a], Ian-Woo Kim [a], Jeonghyeon [b]

[a] Department of Physics, University of Wisconsin, Madison, WI 53706, USA
[b] Division of Quantum Phases & Devices, School of Physics, Konkuk University, Seoul 143-701, Republic of Korea

ARTICLE INFO

Article history:
Received 11 November 2009
Received in revised form 1 September 2010
Accepted 3 September 2010
Available online 17 September 2010
Editor: M. Cvetič

Keywords:
Helicity amplitudes
Models beyond the standard models
Dark matter

ABSTRACT

In many extensions of the SM, neutral massive stable particles (dark matter candidates) are produced at colliders in pairs due to an exact symmetry called a "parity". These particles escape detection, rendering their mass measurement difficult. In the pair production of such particles via a specific ("antler") decay topology, kinematic cusp structures are present in the invariant mass and angular distributions of the observable particles. Together with the end-points, such cusps can be used to measure the missing particle mass and the intermediate particle mass in the decay chain. Our simulation of a benchmark scenario in a Z' supersymmetric model shows that the cusp feature survives under the consideration of detector simulation and the standard model backgrounds. This technique for determining missing particle masses should be invaluable in the search for new physics at the LHC and future lepton colliders.

1. Introduction

Pauli's postulation of a new particle that escapes from detection and carries away energy and angular momentum in β decay not only laid out the foundation for the weak interaction, but also rightfully introduced the first dark matter particle, the neutrino. Ever since then, attempts to determine the masses and other properties of the neutrinos have led to many research efforts in nuclear physics, particle physics, astroparticle physics and cosmology. If the upcoming experiments at the CERN LHC find evidence of large missing energy events beyond the Standard Model (SM) expectations, this exciting discovery may hold the key to explain the missing mass puzzle in the Universe, the dark matter. It is thus of fundamental importance to determine the mass and properties of this missing particle in LHC experiments, to uncover its underlying dynamics and to check its consistency with dark matter expectations.

This task is challenging, however, even with the establishment of missing energy events at the LHC. In hadronic collisions, the undetermined longitudinal motion of the parton-level scattering leads to the ambiguity of their c.m. frame and thus the partonic c.m. energy. Furthermore, with a conserved discrete quantum number (generically called a "parity") that keeps the lightest particle in the new sector stable, the missing particles always come in pairs. The final state kinematics is even less constrained.

Great efforts have been made to reconstruct the mass of the missing particle. It is well known that in cascade decays, the masses of the invisible particles can be extracted from the maximum end-points of kinematic variables such as invariant mass distributions of leptons and jets [1]. Another interesting approach is to determine these parameters from transverse mass variables that utilize missing transverse energy, such as M_{T2} for processes with a pair of missing particles [2]. The end-point of the M_{T2} distribution is known to display a kink when the trial mass for the missing particle is identical to the true mass [3]. For long cascade decay chains, it is possible to determine the unknown masses through the event reconstruction from the mass shell conditions by combining the information from multiple events [4].

In this Letter, we propose an additional method for the missing particle mass measurements, based on what we call "kinematic cusps", non-smooth substructures in kinematic distributions. Kinematic cusps arise in many new physics processes. We focus here on a particular class of processes that we dub as "antler" decays: the two missing parity-odd particles (X) come along with two visible SM particles (a), from the decay of a heavy parity-even particle (D) through intermediate parity-odd particles (B), as shown in Fig. 1. The advantage of considering the kinematic cusps and end-points is that once the parent mass (m_D) is known, the masses of the missing particle (m_X) and the intermediate particle (m_B) can be determined by measuring the energy–momenta of the visible particles without combinatoric complications. Even though the kinematic cusps can be found in other processes, we focus on this

* Corresponding author.
E-mail address: jhsong@konkuk.ac.kr (J. Song).

0370-2693
doi:10.1016/j.physletb.2010.09.010

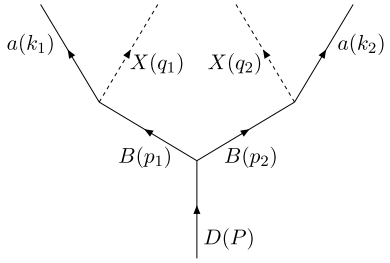

Fig. 1. The "antler" decay diagram, a heavy particle (D) to two visible SM particles (a) and two missing particles (X), via two on-shell intermediate particles (B).

case due to its simplicity. Other examples will be presented elsewhere [5].[1]

The antler topology is common in many scenarios with dark matter particle candidates. Familiar examples can be found in the following theoretically well-motivated models:

$$\begin{aligned}
&\text{MSSM [7]}, && H \to \tilde{\chi}_2^0 + \tilde{\chi}_2^0 \to Z\tilde{\chi}_1^0 + Z\tilde{\chi}_1^0;\\
&Z' \text{ SUSY [8]}, && Z' \to \tilde{\ell}^- + \tilde{\ell}^+ \to \ell^-\tilde{\chi}_1^0 + \ell^+\tilde{\chi}_1^0;\\
&\text{UED [9]}, && Z^{(2)} \to L^{(1)} + L^{(1)} \to \ell^-\gamma^{(1)} + \ell^+\gamma^{(1)};\\
&\text{LHT [10]}, && H \to t_- + t_- \to tA_H + tA_H. \qquad (1)
\end{aligned}$$

The precondition is that the mass of particle D is known a priori. This can be achieved since its even-parity allows its decay into two observable SM particles. In this regard, the antler topology is equally applicable to a lepton collider where the c.m. energy is accurately known. Among these examples above, the decay of Z' in a supersymmetric theory was studied [8] to measure the missing particle mass based on the M_{T2} variable, but the simple and distinctive cusps proposed here were not explored.

For purposes of illustration, we explore two kinematic distributions: (i) M_{aa}, the mass of a_1 and a_2, and (ii) $\cos\Theta$, cosine of the angle between one of the two visible particles and the pair c.m. moving direction in their c.m. frame, as shown in Figs. 2 and 3 for various sets of parameter choice. The distributions have, in addition to the end points, unique non-smooth structures, the cusps (their positions are denoted by vertical lines). While M_{aa} and $\cos\Theta$ are not the only observables displaying the cusp structure, these variables are advantageous since they do not involve the missing transverse energy.

The appearance of the cusp can be understood intuitively as follows. We start with the flat distribution $d^2\Gamma/d\cos\theta_1\, d\cos\theta_2$, where θ_1 and θ_2 are the scattering angles of two visible particles relative to the parent's boost direction in their parent rest frame, and Γ is the partial decay width of the particle D. Any observable can be expressed as a function of (θ_1, θ_2), e.g., $M_{aa}(\theta_1, \theta_2)$. Due to the "antler" decay symmetry, $(\cos\theta_1, \cos\theta_2)$ and $(\cos\theta_2, \cos\theta_1)$ are kinematically equivalent. With this identification, the result of projecting onto M_{aa} is a folded space with three distinctive points or apexes: The lowest apex $(\pm 1, \mp 1)$ and the highest apex $(1, 1)$ correspond to the endpoints $M_{aa}^{\min}$ and $M_{aa}^{\max}$; while the third apex $(-1, -1)$ denotes the position of the cusp, which occurs more frequently than the other two configurations.

Cusps in the antler decay have a number of desirable features in determining the missing particle mass: (i) together with endpoints, cusps can determine both the masses of the intermediate particle B and the missing particle X; (ii) looking for a cusp is statistically advantageous since it has large (in most cases, maximum) event rate; (iii) there is no combinatoric complication due to its simple decay topology; (iv) spin correlations of the decay processes do not change the position of the cusps. In the absence of backgrounds, cusps should be experimentally easy to identify due to their pointed features. In what follows, we will show that the cusp position provides important information about the particle masses in the decay process, which is complementary in many ways to the previously studied mass measurement methods. We will also show that this information is largely retained after the SM backgrounds as well as the detector simulation are included.

[1] General mass measurement techniques using such kinematic singularities have been recently developed [6].

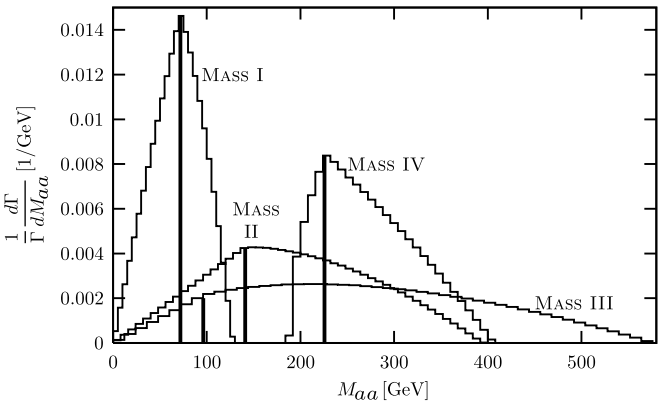

Fig. 2. Normalized differential decay rates versus the invariant mass M_{aa} for various combinations of masses as given in Table 1. The vertical lines indicate the positions of the cusps in each M_{aa} distribution.

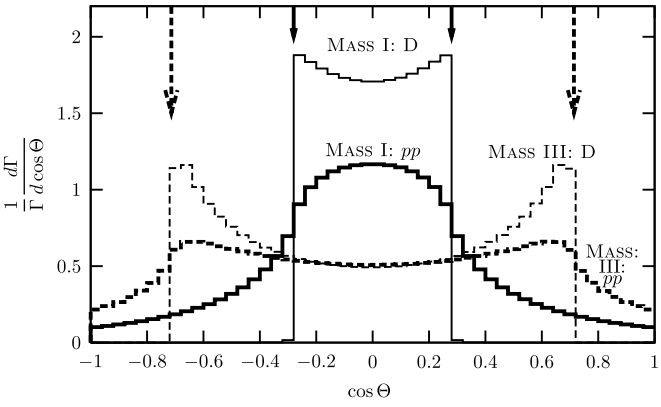

Fig. 3. Normalized differential decay rates versus $\cos\Theta$ in the D-rest frame (thin curves) and in the pp lab frame with $\sqrt{s} = 14$ TeV (thick curves). The parameters of Mass I and Mass III are given in Table 1.

2. Cusp and edge in M_{aa} distribution

We first only show the phase space distributions for on-shell particles. It is convenient to use the rapidities: the rapidity η of particle B and the rapidity ζ of particle a in the rest frames of their parents D and B, respectively. The rapidities η and ζ are given by

$$\cosh\eta = \frac{m_D}{2m_B} \equiv c_\eta, \qquad \cosh\zeta = \frac{m_B^2 - m_X^2 + m_a^2}{2m_a m_B} \equiv c_\zeta.$$

Here and henceforth we use a shorthand notation of $c_x \equiv \cosh x$. Obtaining the rapidities would be equivalent to measuring the masses m_B and m_X.

(1) $m_a = 0$ *case*: Consider a to be massless first for simplicity. One would naively expect the invariant mass to have an end-point $M_{aa}^{\max} = m_D - 2m_X$. However, due to the on-shell constraint for the particle B, we find a different end-point:

Table 1
Test mass spectrum sets for mass measurements using kinematic cusp structure (m_Z is the Z boson mass).

	m_D (GeV)	m_B (GeV)	m_a (GeV)	m_X (GeV)
Mass I	1250	600	0	550
Mass II	1000	440	0	300
Mass III	1000	350	0	200
Mass IV	600	250	m_Z	100

$$M_{aa}^{\max} = m_B\left(1-\frac{m_X^2}{m_B^2}\right)e^{\eta}. \tag{2}$$

In addition, the M_{aa} distribution has a cusp at

$$M_{aa}^{\text{cusp}} = m_B\left(1-\frac{m_X^2}{m_B^2}\right)e^{-\eta}. \tag{3}$$

This is remarkable since the ratio $M_{aa}^{\max}/M_{aa}^{\text{cusp}} = e^{2\eta}$ is governed by the initial decay $D \to BB$ and thus gives m_B. The product $M_{aa}^{\max}M_{aa}^{\text{cusp}}$ depends on the secondary decay $B \to aX$ and gives m_X. Furthermore, $d\Gamma/dM_{aa}$ is

$$\frac{d\Gamma}{dM_{aa}} \propto \begin{cases} 2\eta M_{aa}, & \text{if } 0 \leqslant M_{aa} \leqslant M_{aa}^{\text{cusp}}; \\ M_{aa}\ln\frac{M_{aa}^{\max}}{M_{aa}}, & \text{if } M_{aa}^{\text{cusp}} \leqslant M_{aa} \leqslant M_{aa}^{\max}. \end{cases} \tag{4}$$

Fig. 2 shows $d\Gamma/dM_{aa}$ for four sets of representative masses specified in Table 1. The choice of the parameters for Mass I is motivated by the $Z^{(2)}$ decay in the UED model [9]. Since the two subsequent decays $Z^{(2)} \to L^{(1)}L^{(1)}$ and $L^{(1)} \to \ell\gamma^{(1)}$ occur near the mass threshold, Mass I is to be called the "near threshold case". For comparison, we consider the mass parameters with sizable gap in Mass III, the "large mass gap case." The visibility of the cusp depends on the ratio $M_{aa}^{\text{cusp}}/M_{aa}^{\max}$. As shown in Eq. (4), the distribution for $M_{aa} < M_{aa}^{\text{cusp}}$ is linear, while that after M_{aa}^{cusp} is a concave curve with the maximum at $M_{aa}^{\max}/e$. The cusp becomes a sharper peak if $M_{aa}^{\text{cusp}} \geqslant M_{aa}^{\max}/e$ (or equivalently $m_B > 0.44m_D$). The parameters in Mass II are chosen to represent this boundary case of $m_B \approx 0.44m_D$. The cusp structure is more pronounced for the near threshold case (Mass I) than the large mass gap case (Mass III).

(2) $m_a \neq 0$ *case*: If the SM particle a is massive (a Z boson or a top quark), we call it the "massive case". The parameter choice in Mass IV, motivated by the MSSM heavy Higgs boson decay associated with two SM Z bosons, is an example. In this case, the analytic form of $d\Gamma/dM_{aa}$ is given by three pieces (the explicit forms are not very illuminating and thus not given here). Its maximum is

$$M_{aa}^{\max} = 2m_a c_{\eta+\zeta}. \tag{5}$$

The positions of $M_{aa}^{\min}$ and M_{aa}^{cusp} are as follows, depending on the relations of the two rapidities η and ζ:

	$\eta < \zeta/2$	$\zeta/2 < \eta < \zeta$	$\zeta < \eta$
$M_{aa}^{\min}$	$2m_a$	$2m_a$	$2m_a c_{\eta-\zeta}$
M_{aa}^{cusp}	$2m_a c_{\eta-\zeta}$	$2m_a c_\eta$	$2m_a c_\eta$

(6)

For all three regions in Eq. (6), the M_{aa} distribution shows a sharp cusp, as illustrated by the Mass IV case in Fig. 2. Note that the case $\zeta < \eta$ has different $M_{aa}^{\min}$, rather than $2m_a$ as naively expected. It is due to the enhanced boost of the two fast-moving parent B's. This shift helps to resolve the ambiguity among the three regions. Still a two-fold ambiguity in the $\eta < \zeta/2$ and $\zeta/2 < \eta < \zeta$ regions remains since we do not know whether the measured M_{aa}^{cusp} is $2m_a c_{\eta-\zeta}$ or $2m_a c_\eta$.

We propose another independent observable to break this ambiguity, $(\Delta|p_T^a|)_{\max}$, which is the maximum of the difference between the magnitudes of the two transverse momenta of a_1 and a_2:

$$\begin{aligned}\left(\Delta\left|p_T^a\right|\right)_{\max} &\equiv \max\left(\left|\vec{p}_T^{\,a_1}\right| - \left|\vec{p}_T^{\,a_2}\right|\right) \\ &= m_a\left[\sinh(\eta+\zeta) - \sinh|\eta-\zeta|\right],\end{aligned} \tag{7}$$

which is invariant under longitudinal boosts. Note that the two-fold ambiguity happens when $\eta < \zeta$. With the observed $M_{aa}^{\max}$ and $M_{aa}^{\min}$, $(\Delta|p_T^a|)_{\max}$ provides independent information.

3. Cusp in angular distribution

We also have analyzed the distribution with respect to $\cos\Theta$, where Θ is the angle of a visible particle, say a_1, in the c.m. frame of a_1 and a_2, with respect to their c.m. moving direction. The expression of $d\Gamma/d\cos\Theta$ in the D-rest frame for $m_a = 0$ is remarkably simple:

$$\frac{d\Gamma}{d\cos\Theta} \propto \begin{cases} \sin^{-3}\Theta, & \text{if } |\cos\Theta| \leqslant \tanh\eta, \\ 0, & \text{otherwise.} \end{cases} \tag{8}$$

The distribution has a sharp end-point, another cusp, with the highest event rate at the boundary:

$$|\cos\Theta|_{\max} = \tanh\eta = \sqrt{1-4m_B^2/m_D^2}. \tag{9}$$

While this variable is unambiguous in the lab frame at a lepton collider, we cannot determine the longitudinal motion of the particle D in a hadron collider. After convoluting with the parton distribution functions, $d\Gamma/d\cos\Theta$ is smeared. In Fig. 3, we compare the $\cos\Theta$ distribution in the rest frame of D (thin curves) with that in the lab frame at the LHC (thick curves) for the near threshold case (Mass I) and the large mass gap case (Mass III). We have assumed that D is produced by direct s-channel gg or $q\bar{q}$ annihilation so that the longitudinal momentum distribution of D is obtained from the parton distribution of the incident protons.

The convolution effects with the partons smear out the sharp $\cos\Theta$ cusp in the lab frame. For the near threshold case (Mass I), the two sharp rises at both ends get much less pronounced, although it is still possible to read the edge point off in the distribution. For the large mass gap case (Mass III), as the end point position approaches towards $\cos\Theta = \pm 1$, the sharpness of two cusps maintains better. It is interesting to note that the cusp in the M_{aa} distribution and that in the $\cos\Theta$ distribution provide complementary information for determining m_B. The invariant mass distribution yields a better resolution for the near threshold case, while the angular distribution provides better one for the large mass gap case.

To some extent, the $\cos\Theta$ distribution in the D-rest frame may be obtained even in hadron collisions. The smearing effects can be effectively modeled by the well-known parton distribution functions in the large x region. Or the direct resonant decay of D into SM particles allows to extract the velocity distribution of D, which can be used to recover $d\Gamma/d\cos\Theta$ in the D-rest frame.

4. Discussion

To this point, the discussions on the kinematic cusps are rather theoretical, i.e., considering only the kinematics at parton level with perfect mass shell conditions, and ignoring the SM backgrounds as well as the detector simulation. First we consider the effects of the matrix elements regarding the spin correlations between the initial state and final state particles. We have confirmed that, for the four processes in Eq. (1), including the full matrix

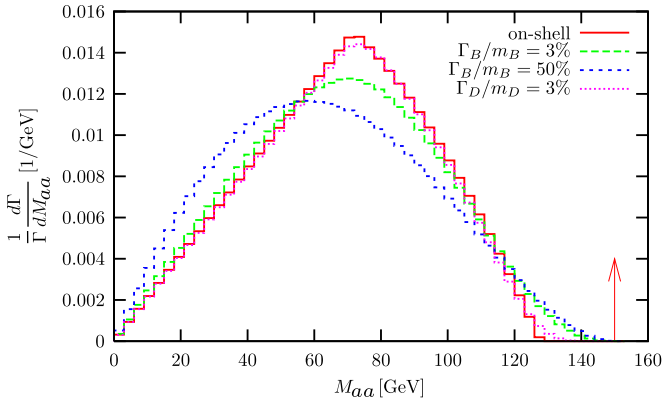

Fig. 4. The invariant mass distribution for the MASS I case: $m_D = 1250$ GeV, $m_B = 600$ GeV, with the finite decay widths $\Gamma_D/m_D = 3\%$ (dotted), and $\Gamma_B/m_B = 3\%$, 50% (long dashed and short dashed) respectively.

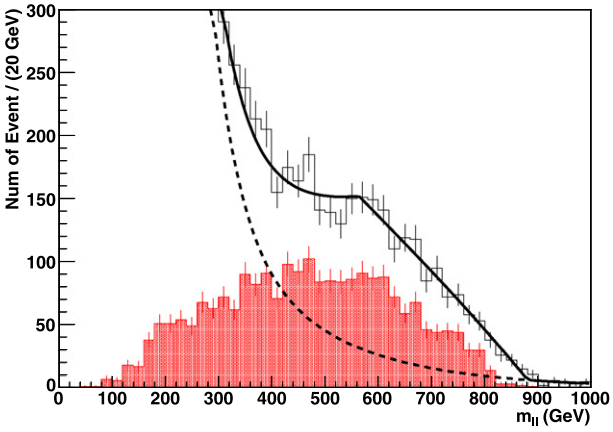

Fig. 5. Event distribution of the di-lepton invariant mass for the signal $Z' \to \tilde{\ell}^+\tilde{\ell}^- \to \ell^+\ell^-\chi_1^0\chi_1^0$ as well as the SM backgrounds at the 14 TeV LHC and 100 fb^{-1}. The upper histogram with statistical error bars: signal plus background with $\not{E}_T > 50$ GeV; the dotted curve for SM background only with $\not{E}_T > 50$ GeV. Shaded histogram: signal with $\not{E}_T > 200$ GeV. Mass parameters are given in Eq. (10).

elements does not change the shape of the distributions. The deviations from the phase space predictions become appreciable when the fermions and vector bosons (like the $Z^{(2)}$ in UED) have chiral couplings for both $D \to BB$ and $B \to aX$ decays. Even in this extreme case, the cusped peak remains at the same location and its height is changed by about 2%.

However, non-vanishing decay widths of the parent and intermediate particles can alter the shape of the distributions. In Fig. 4, we show the M_{aa} distributions for different finite decay widths Γ_B and Γ_D in the MASS I spectrum. Finite Γ_D has much milder effect than Γ_B. With $\Gamma_B/m_B = 3\%$, the finite decay width effect changes the distribution shape and the position of $M_{aa}^{\max}$, while essentially keeping the M_{aa}^{cusp} position. For illustration, we also show a very broad case $\Gamma_B/m_B = 50\%$. This nearly off-shell situation smears the triangular cusp shape considerably. The momenta of the visible particles span all of the allowed phase space given by m_D and m_X, regardless of m_B. The maximum of M_{aa} approaches $m_D - 2m_X$, denoted by the arrow in Fig. 4. The end point measurement with the known m_D leads to the missing particle mass m_X, just like the direct neutrino mass determination in tritium decays. In the real scenarios listed in Eq. (1), the intermediate particles ($\tilde{\chi}_2^0$, $\tilde{\ell}^\pm$, $L^{(1)}$ and t_-) typically have decay widths smaller than one percent of their masses. The M_{aa} cusp shape remains intact.

We next explore to what extent the SM backgrounds and detector effects at the LHC would degrade the sharp cusps. We consider a benchmark scenario in a SUSY model with an extra $U(1)$ gauge boson Z' [11]. In a minimal model where there is no mixing between Z' and the SM gauge bosons, the only relevant interactions of Z' are with the SM fermions and their SUSY partners, through the interaction Lagrangian $\mathcal{L} \supset g_1' Y_f \bar{f}\gamma^\mu f Z'_\mu$. Our signal process is $Z' \to \tilde{\ell}^-\tilde{\ell}^+ \to \ell^-\tilde{\chi}_1^0\ell^+\tilde{\chi}_1^0$ with the mass parameters

$$(m_{Z'}, m_{\tilde{\ell}}, m_{\chi_1^0}) = (1500, 730, 100)\ \text{GeV}. \tag{10}$$

To manifest our signal, we take an optimistic scenario where $g_1' = 0.63$, $Y_{\text{quark}} = Y_{\text{lepton}}/2 = 1$, and all the sfermions except for $\tilde{e}_{L,R}^\pm$ and $\tilde{\mu}_{L,R}^\pm$ are heavier than $m_{Z'}/2$.

The signal is two leptons with missing transverse energy. The leading irreducible SM backgrounds are $W^+W^-/ZZ \to \ell^+\ell^-\nu\bar{\nu}$. The $t\bar{t}$ backgrounds decaying into $b\bar{b}\ell^+\ell^-\nu\bar{\nu}$ can be dominant if not imposing very strong acceptance cuts. The SUSY backgrounds in this scenario are expected to be small: (i) the slepton pair production followed by the decay of $\tilde{\ell}^\pm \to \ell^\pm\tilde{\chi}_1^0$ is suppressed by the P-wave suppression and the heavy slepton mass, leading to the total cross section of ~ 0.7 fb for the mass parameters in Eq. (10); (ii) another SUSY background of $pp \to \tilde{\chi}^+\tilde{\chi}^- \to \ell^+\tilde{\nu}\ell^-\tilde{\nu}$ is extremely small because $m_{\tilde{\nu}} \gg m_{\tilde{\chi}_1^\pm}$ in this scenario; (iii) finally the rate of $pp \to \tilde{\chi}^+\tilde{\chi}^- \to W^+W^-\tilde{\chi}_1^0\tilde{\chi}_1^0$ followed by the leptonic decay of $W^\pm$ is also suppressed in the Bino LSP scenario. Therefore we ignore the SUSY background in what follows.

To suppress the SM top quark background, we veto the additional hard jets in the kinematic region

$$E_j > \begin{cases} 50\ \text{GeV} & \text{if } 3 < |\eta_j| < 5, \\ 25\ \text{GeV} & \text{if } |\eta_j| < 3, \end{cases} \tag{11}$$

where η_j is the jet pseudo-rapidity. We have used `MadGraph/MadEvent/PYTHIA` [12] for the event generation and `PGS` [13] for detector simulation.

In Fig. 5, we show the lepton invariant mass distribution of the Z' antler decay signal over the SM backgrounds through WW, WZ, ZZ and $t\bar{t}$ processes at the LHC with c.m. energy 14 TeV and luminosity 100 fb^{-1}. The upper histogram with statistical error bars presents the signal plus backgrounds for $\not{E}_T > 50$ GeV, and the dotted line is the SM background only. The SM background (especially $t\bar{t}$ ones) can still be substantial and comparable to the signal, although the cusp feature and position can be clearly visible over the continuous background. The shaded histogram shows the signal for $\not{E}_T > 200$ GeV, and the SM background is essentially invisible with this stringent missing energy cut. Although the signal can be made way above the SM background with the characteristic solitary triangular shape, the severe missing $\not{E}_T$ cut alters the position of endpoint and smears the shape of the cusped peak. This is because the singly-produced heavy Z' has little transverse motion, and the two missing particles are back-to-back for the cusp and the end-point configurations, corresponding to low $\not{E}_T$ situation. Some optimal treatment is needed with respect to the selective kinematic cuts in order to effectively extract the missing particle mass.

Once the signal is established with various cuts, we analyze the events with the low $\not{E}_T$ cut (which faithfully respect the original cusp kinematics), and apply the known theoretical function in Eq. (4). The best fit to the data curve leads to the reconstructed mass parameters as

$$m_{\tilde{\ell}}^{\text{recon}} = 731.7^{+2.1}_{-5.2}\ \text{GeV},$$
$$m_{\chi_1^0}^{\text{recon}} = 142.0^{+24.1}_{-39.7}\ \text{GeV}.$$

While the $\tilde{\ell}$ mass is determined with an impressive accuracy, better than a percent, the neutralino mass is significantly shifted, with about a 50% error. This uncertainty once again is mainly due to the distortion from $\not{E}_T$ cut.

5. Conclusions

New techniques to measure the missing particle mass at the LHC are proposed based on an antler decay topology ($D \to BB \to aXaX$), with a final state of two visible particles a and two missing particles X via intermediate particles B. We found a new type of kinematical singularity structure, the cusps in the invariant mass distribution of two visible particles and an angular distribution. Its pure kinematical origin renders its cusp position and the distribution shape nearly intact under the influence of the dynamical matrix elements. Along with the end points of the distributions, the cusps can determine the missing particle mass as well as the intermediate particle mass. We demonstrated in a realistic example including the SM background analysis and detector simulations that the signal is observable and the masses can be determined to a reasonable accuracy.

Our proposal relies on the observation of the antler decay, which are motivated in many new physics models. If such processes are seen in colliders, this method will provide a new way for mass measurement. We believe that this technique will be invaluable for searches for new physics at the LHC and future lepton colliders, as well as in any other processes with similar kinematics. The missing mass determination at colliders would undoubtedly shed light on the direct and indirect dark matter searches.

Acknowledgements

This work is supported in part by the U.S. Department of Energy under grant No. DE-FG02-95ER40896. The work of J.S. was supported by the WCU program through the KOSEF funded by the MEST (R31-2008-000-10057-0).

References

[1] I. Hinchliffe, F.E. Paige, M.D. Shapiro, J. Soderqvist, W. Yao, Phys. Rev. D 55 (1997) 5520;
B.C. Allanach, C.G. Lester, M.A. Parker, B.R. Webber, JHEP 0009 (2000) 004;
B.K. Gjelsten, D.J. Miller, P. Osland, JHEP 0412 (2004) 003;
M. Burns, K.T. Matchev, M. Park, JHEP 0905 (2009) 094;
K.T. Matchev, F. Moortgat, L. Pape, M. Park, arXiv:0906.2417.
[2] C.G. Lester, D.J. Summers, Phys. Lett. B 463 (1999) 99;
A. Barr, C. Lester, P. Stephens, J. Phys. G 29 (2003) 2343;
C. Lester, A. Barr, JHEP 0712 (2007) 102;
P. Konar, K. Kong, K.T. Matchev, JHEP 0903 (2009) 085.
[3] W.S. Cho, K. Choi, Y.G. Kim, C.B. Park, Phys. Rev. Lett. 100 (2008) 171801;
B. Gripaios, JHEP 0802 (2008) 053;
W.S. Cho, K. Choi, Y.G. Kim, C.B. Park, JHEP 0802 (2008) 035;
A.J. Barr, B. Gripaios, C.G. Lester, JHEP 0802 (2008) 014.
[4] M.M. Nojiri, G. Polesello, D.R. Tovey, arXiv:hep-ph/0312317;
K. Kawagoe, M.M. Nojiri, G. Polesello, Phys. Rev. D 71 (2005) 035008;
H.C. Cheng, J.F. Gunion, Z. Han, G. Marandella, B. McElrath, JHEP 0712 (2007) 076;
H.C. Cheng, D. Engelhardt, J.F. Gunion, Z. Han, B. McElrath, Phys. Rev. Lett. 100 (2008) 252001.
[5] T. Han, I.W. Kim, J. Song, in preparation.
[6] I.W. Kim, arXiv:0910.1149 [hep-ph].
[7] A. Djouadi, Phys. Rep. 459 (2008) 1.
[8] M. Baumgart, T. Hartman, C. Kilic, L.T. Wang, JHEP 0711 (2007) 084.
[9] A. Datta, K. Kong, K.T. Matchev, Phys. Rev. D 72 (2005) 096006;
A. Datta, K. Kong, K.T. Matchev, Phys. Rev. D 72 (2008) 119901 (Erratum);
H.C. Cheng, K.T. Matchev, M. Schmaltz, Phys. Rev. D 66 (2002) 036005.
[10] A. Freitas, P. Schwaller, D. Wyler, arXiv:0906.1816.
[11] L. Basso, A. Belyaev, S. Moretti, G.M. Pruna, C.H. Shepherd-Themistocleous, arXiv:1002.3586 [hep-ph].
[12] F. Maltoni, T. Stelzer, JHEP 0302 (2003) 027, arXiv:hep-ph/0208156;
T. Sjostrand, S. Mrenna, P.Z. Skands, JHEP 0605 (2006) 026, arXiv:hep-ph/0603175.
[13] http://www.physics.ucdavis.edu/~conway/research/software/pgs/pgs4-general.htm.